# A Hierarchical Classification Scheme of Psoriasis Images

Gabriela Maletti and Bjarne Ersbøll

Department of Informatics and Mathematical Modelling,
Technical University of Denmark,
DK-2800 Kgs. Lyngby, Denmark
{gmm, be}@imm.du.dk
http://www.imm.dtu.dk/image

**Abstract.** A two-stage hierarchical classification scheme of psoriasis lesion images is proposed. These images are basically composed of three classes: normal skin, lesion and background. The scheme combines conventional tools to separate the skin from the background in the first stage, and the lesion from the normal skin in the second stage. These tools are the Expectation-Maximization Algorithm, the quadratic discrimination function and a classification window of optimal size. Extrapolation of classification parameters of a given image to other images of the set is evaluated by means of Cohen's Kappa coefficient.

## 1 Introduction

We use a set of 175 *RGB* psoriasis lesions images, of size 556 pixels by 748 pixels, taken at the Gentofte Hospital, Denmark, during pilot sessions with three invited patients. For each patient, three lesions were followed once a week during at least three weeks. In each session, five images of each lesion were taken. Examples can be seen in Figure 1.

The images of lesions with psoriasis can be assumed to contain three classes: background, normal skin and lesion. Lesions have high contrast with the rest of the image in the third principal component. Principal Component Analysis has shown that a rough estimation of the third component can be obtained subtracting the green band from the blue band, while the red band almost does not have any influence [6]. Alternatively, in the absolute difference $|B - G|$, lesions and background are both enhanced from the normal skin. The background has a good contrast with the rest in the red band: advantage can be taken of the green color of the curtain used as background during the image acquisition process, because its density function is positioned in one extreme of the red band histogram.

The present classification scheme consists of two stages. In the first stage, the skin is separated from the background using the red band, and, in the second stage, the lesion is separated from the normal skin using the absolute value of

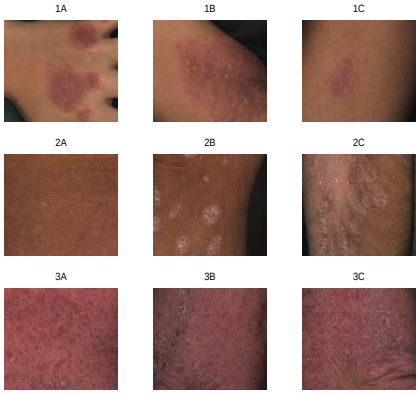


**Fig. 1.** Set of Psoriasis Lesions. From top to bottom, the row number corresponds with the patient number. From left to the right, columns correspond to the labelled lesions $A$, $B$ and $C$, respectively.

the difference between the blue and the green bands.

For future alignment purposes, it is expected that, for a given lesion, the classification scheme produces thematic maps with a repeated pattern indicating that lesion within and between sessions.

## 2 Lesion Classification

As mentioned before, the hierarchical classification scheme is composed of two stages. In both steps, the pixels of the classes are assumed to be Gaussian distributed. Although this is almost certainly not the case, Clarke et al. have shown that the quadratic method is fairly robust to deviations from normality, unless we have very skewed marginals [2]. The red band $R$ is first used to discriminate between the background and the skin, then the output of the previous step is combined with the $|B - G|$ band for segmenting the lesions from the normal skin. In both stages, the use of Wang's Expectation-Maximization Algorithm [11] (setting $\epsilon = 0.0001$ in [11]) is proposed. This algorithm is expected to provide the parameters (mean $\mu$, covariance matrix $\Sigma$ and a-priori probability $p$) of two Gaussian distributed classes: skin and background in the first step, and lesions and normal skin in the second step. The threshold between the classes is obtained using the following discrimination function for Gaussian distributed classes with different dispersion [3]:

$$-(x-\mu_1)'\Sigma_1^{-1}(x-\mu_1)+(x-\mu_2)'\Sigma_2^{-1}(x-\mu_2)\geq 2log(\frac{L_{(2,1)}p_2}{L_{(1,2)}p_1}) \quad (1)$$

where $\mu_i$ is the mean, $\Sigma_i$ is the covariance matrix and $p_i$ is the a priori probability of the $i-th$ class $\forall i \in \{1,2\}$. $L_{(1,2)}$ is the cost of belonging to class 1 and being classified as belonging to class 2 and vice-versa for $L_{(2,1)}$.

The discrimination function is applied to the output of the convolution of the image with a circular window of optimal size. The critical number of elements needed for classification is computed as a function of the minimal separability between the two classes [7]:

$$w_{(1),(2)} = -6.8341 + \frac{7.1800}{\sqrt{dA_{(1),(2)}}} \quad (2)$$

where $w$ is the radius of the estimated optimal disc for classification and $dA$ is the weighted sum of the difference of areas of the class density functions:

$$dA_{(1),(2)} = dA_{(1),(2)} = \frac{1}{2}\sum_{n=1}^{Q}|h_{(1)}[n]-h_{(2)}[n]| \quad (3)$$

$Q$ is the number of quantization levels, $h_{(1)}$ and $h_{(2)}$ are the estimated density functions of classes 1 and 2 respectively.

The values of this optimal window sum to one; each element of the window has the value $1/n_c$ corresponding to the inverse of the size of the window $n_c$ given by its number of elements. It is clear that after convolving the image, each pixel is replaced with the estimated mean of its neighborhood.

In the first step of this classification scheme, pixels whose estimated local mean is greater than the threshold are considered belonging to the class skin, and vice-versa, for the background. In the second step, pixels whose estimated mean of the neighborhood is greater than the threshold are considered belonging to the class normal skin, and vice-versa, for the lesion. Note that, in both cases, the discrimination function is constructed with the original data, but it is applied to the pixels belonging to the output of the convolution. A set of thematic maps indicating the clases, the lesions and the rest, is obtained at the end of this stage.

### 2.1 Results and Discussion

During the classification stage: for the first step, the costs were $L_{(A,B)} = 500$ and $L_{(B,A)} = 1$; for the second step, $L_{(A,B)} = 1$ and $L_{(B,A)} = 1$ was set. These

values were empirically found. Setting individual parameters depending on the lesions could obviously improve the results obtained. However, to set the same values for all the cases was helpful for comparison purposes. The Expectation-Maximization Algorithm was applied to each single image. Classification outputs are presented for each single image and classification stage in Appendix A.

By visual assessment of the classification output of the first stage, it can be noted that the results are satisfactory, except for the set of images of the third session of the case $(2, C)$, which is a lesion partially covered by hair. With regard to the output of the second classification stage, which is the desired output, comments to each particular case follow. For the first patient, the output of the classification scheme proposed has shown to be enough to define a smaller searching and alignment area of the lesion patterns with satisfactory results, in spite of some border effects produced by the window size. On the other hand, it could be said that for the case $(2, A)$ the expected common pattern roughly appears in the thematic maps, however, it does not correspond to the lesion. The shadows present on the image borders clearly are influencing the classification results. In fact, the presence of shadows did not affect the output of the first classification stage very much, which contained for a given lesion, a repeated skin pattern within and between sessions. However, it clearly affects the output of the second classification stage for the cases $(2, B)$, $(2, C)$, $(3, A)$, $(3, B)$ and $(3, C)$.

An aspect that has to be put under consideration during the alignment process, is the size of the lesion pattern. By visual inspection of the original data-set, it can be deduced that the size between lesions has a significant variance: in some images, one clear lesion composed by only one connected region can be observed, while in other cases, a lesion can consist of a set of smaller size connected regions; finally, there are also examples, where the number of connected regions is so large while the size of the regions is so small, that the whole can be taken as only one lesion. It is clear that a good definition of the lesion does not avoid the illumination problem.

In order to reduce the processing time, one aspect considered was the use of the output of the first image of each session as input for the remaining images of the session. In the following, the uncertainty of using the parameters of a randomly selected image for a given patient, lesion and session, to segment the remaining images of the same session is evaluated. Since the images are not registered, a descriptor that is invariant to translations and rotations is required. This is the case of the normalized histogram. Table 1 is based on data presented in Table 4. Each single $\mu$ cell value in Table 1 was computed according to the following Equation:

$$\mu_{p,l,s} = \frac{1}{n_c} \sum_{i=1}^{n_c} E[c[h_{p,l,s,i,b}, h_{p,l,s,:,b}]] \tag{4}$$

where $E[corr(h(nX_{p,l,s,i,b}), h(nX_{p,l,s,:,b}))]$ is calculated using Equation 13 and $p$ is the index for patient, $l$, for lesion, $s$, for session, $i$, for capture, $b$ for color band. The symbol $n_c$ is the number of captures of the $s-th$ session. The session $s$ takes values in {'a','b','c','d'}, where the order in the sequence indicates the session week. The color band $b$ takes values in {'R','G','B'}.

In a similar fashion, for the standard deviation, each single $\sigma$ cell value is obtained by computing the following:

$$\sigma_{p,l,s} = \sqrt{\frac{1}{n_c}\sum_{i=1}^{n_c}(E[c[h_{p,l,s,i,b}, h_{p,l,s,:,b}]] - \mu_{p,l,s})^2} \tag{5}$$

where the indexes have the same meaning as in Equation 4.

**Table 1.** Average and dispersion correlation value between the normalized histogram of a normalized image red band and the normalized histogram of the normalized red bands of the images belonging to the same session.

| (Patient, Lesion) | $\mu_a$ | $\sigma_a$ | $\mu_b$ | $\sigma_b$ | $\mu_c$ | $\sigma_c$ | $\mu_d$ | $\sigma_d$ |
|---|---|---|---|---|---|---|---|---|
| (1,A) | 0.8525 | 0.0260 | 0.8618 | 0.0328 | 0.8521 | 0.0391 | 0.8448 | 0.0258 |
| (1,B) | 0.8055 | 0.0248 | 0.8107 | 0.0348 | 0.7264 | 0.0210 | 0.7342 | 0.0305 |
| (1,C) | 0.8413 | 0.0061 | 0.8876 | 0.0192 | 0.8650 | 0.0156 | | |
| (2,A) | 0.7991 | 0.0113 | 0.8777 | 0.0174 | 0.8486 | 0.0215 | 0.8774 | 0.0673 |
| (2,B) | 0.8937 | 0.0110 | 0.7312 | 0.0438 | 0.8326 | 0.0100 | 0.8841 | 0.0464 |
| (2,C) | 0.8345 | 0.0151 | 0.7924 | 0.0231 | 0.8535 | 0.0145 | 0.7906 | 0.0514 |
| (3,A) | 0.8477 | 0.0094 | 0.9072 | 0.0155 | 0.8675 | 0.0204 | 0.8731 | 0.0186 |
| (3,B) | 0.7708 | 0.0372 | 0.8776 | 0.0292 | 0.7498 | 0.0310 | 0.9062 | 0.0329 |
| (3,C) | 0.8749 | 0.0265 | 0.9057 | 0.0098 | 0.8799 | 0.0362 | 0.8074 | 0.0233 |

Table 2 was constructed in the same fashion as in Table 1, but using the skin data of the |B-G| band.

Results presented in Tables 1 show that in general, the normalized histograms of red bands of images belonging to the same sessions are have a correlation superior to 0.8. Exceptions are, for instance, the cases for which the lesion presents occlusions. See the last captures of the the third and fourth session of the case $(1, B)$. See also the first and fifth capture of the second session of the case $(2, B)$. Note that in the first session of the case $(3, B)$, the two last captures show a large translation on the focused region. For the images of the third session of the case $(3, B)$, it can be observed that the shadows are not presented in the same way, for all the captures. Shadows, hairs and occlusions seem not to be irrelevant.

With regard to the results presented in Table 2, which was generated using only the values of pixels belonging to the class skin, it has to be mentioned,

**Table 2.** Average and standard deviation correlation value between the normalized histogram of a normalized $|B-G|$ band skin data and the normalized histogram of the normalized $|B-G|$ bands skin data of the images belonging to the same session.

| (Patient, Lesion) | $\mu_a$ | $\sigma_a$ | $\mu_b$ | $\sigma_b$ | $\mu_c$ | $\sigma_c$ | $\mu_d$ | $\sigma_d$ |
|---|---|---|---|---|---|---|---|---|
| (1,A) | 0.6472 | 0.0819 | 0.5790 | 0.0353 | 0.5011 | 0.1946 | 0.5387 | 0.0735 |
| (1,B) | 0.6170 | 0.1594 | 0.7657 | 0.1718 | 0.3759 | 0.0752 | 0.5461 | 0.0437 |
| (1,C) | 0.6166 | 0.1483 | 0.7061 | 0.0502 | 0.6569 | 0.0272 | | |
| (2,A) | 0.7306 | 0.0474 | 0.6279 | 0.0227 | 0.6916 | 0.1287 | 0.6956 | 0.0678 |
| (2,B) | 0.5881 | 0.1014 | 0.5786 | 0.1156 | 0.5373 | 0.0678 | 0.6598 | 0.1591 |
| (2,C) | 0.5877 | 0.1490 | 0.5755 | 0.1130 | 0.6440 | 0.1524 | 0.6296 | 0.1287 |
| (3,A) | 0.6199 | 0.0732 | 0.6602 | 0.0604 | 0.5344 | 0.0787 | 0.5798 | 0.0727 |
| (3,B) | 0.6797 | 0.0457 | 0.5004 | 0.0695 | 0.4920 | 0.1040 | 0.4405 | 0.0782 |
| (3,C) | 0.8134 | 0.1557 | 0.7117 | 0.0653 | 0.7988 | 0.1681 | 0.5462 | 0.0851 |

that the average correlation values decrease for all the cases, which is not very encouraging. However, as mentioned before, there is more contrast between the lesion and the rest in these bands.

The application of the discrimination function generated with the parameters produced by the Expectation-Maximization Algorithm for the first image of each session to the remaining images of the same session is evaluated here. Cohen's Kappa coefficient [9], [10] was used to compare pairs of thematic maps produced for each given single image. For each pair, the first thematic map was produced with the discrimination function depending on the given image data. The second thematic map was produced with the discrimination function of the first image of the session the given image belongs to. For each pair, the first thematic map was used as the ground truth. The Kappa coefficient is a global indicator of classification quality, which varies from minus one to one, where a perfect classification would give a value of one, and a completely erroneous classification would give a value of minus one. For each pair of corresponding thematic maps, the confusion matrix $C$ [5] was constructed assuming two classes ($k = 2$). For the first classification stage, these classes were the curtain and the skin. For the second classification stage, the normal skin and the lesion.
The Kappa coefficient is defined as:

$$\kappa = \frac{(d-q)}{N-q} \tag{6}$$

where

$$d = \sum_{i=1}^{k} c_{i,i}$$
$$q = \frac{\sum_{i=1}^{k}((\sum_{j=1}^{k} c_{i,j})(\sum_{j=1}^{k} c_{i,j}))}{N} \tag{7}$$
$$N = \sum_{i=1}^{k}\sum_{j=1}^{k} c_{i,j}$$

and $c_{i,j}$ is the element of the confusion matrix located at the $i-th$ row and $j-th$ column.

Each single cell value in Tables 6 and 7 is a Kappa value $\kappa_{p,l,s,c,r}$ where $p$ means patient, $l$, lesion, $s$, session, $c$, capture and $r$ is for Table 6 equal to "SKIN" and for Table 7 equal to "LESION".

The average and standard deviation of the Kappa coefficient was computed for each patient and lesion, first using the thematic maps indicating skin (the output of the first classification stage), and then using the thematic maps indicating lesions (the output of the second classification stage). The estimation of the average of Kappa is defined as:

$$E[\kappa_{p,l,r}] = \frac{1}{n_s(n_c-1)} \sum_{s=1}^{n_s}\sum_{c=2}^{n_c} \kappa_{p,l,s,c,r} \tag{8}$$

where $p$ is the patient, $l$, the lesion, $s$, the session, $c$ the capture and $r$ takes values in $\{'SKIN','LESION'\}$. Note that the Kappa value of the first image of each session is not included, because it is supposed to be one. The standard deviation of $\kappa_{p,l,r}$ is defined as:

$$S[\kappa_{p,l,r}] = \sqrt{\frac{1}{n_s(n_c-1)} \sum_{s=1}^{n_s}\sum_{c=2}^{n_c} \kappa^2_{p,l,s,c,r} - E^2[\kappa_{p,l,r}]}. \tag{9}$$

Results can be seen in Table 3, which is based on data of Tables 6 and 7.

Excluding the six captures where the lesion $(1,B)$ is occluded (the last two captures from the second to the fourth session), the mean Kappa (see Equation 8) increases from 0.7805 to 0.9081 and from 0.6687 to 0.8769, and its standard deviation reduces from 0.1974 to 0.0601 and from 0.3223 to 0.0969, for the first and second classification stage respectively[1]. The bad classification outputs in the case $(2,C)$ are partly due to the fact that the lesion is partially covered by hair. On the other hand, by visual assessment of the incomplete thematic maps

[1] See in [8] a scheme for registration in presence of occlusions.

**Table 3.** Classification Stage: Kappa values $\kappa$ of the classification outputs using the parameters of each single image compared with the classification output by using the parameters of the first image of each session.

$N$ is the number of processed images.

| (Patient, Lesion) | N | $E[\kappa_{p,l,SKIN}]$ | $S[\kappa_{p,l,SKIN}]$ | $E[\kappa_{p,l,LESION}]$ | $S[\kappa_{p,l,LESION}]$ |
|---|---|---|---|---|---|
| (1,A) | 20 | 0.9171 | 0.0580 | 0.8966 | 0.0710 |
| (1,B) | 20 | 0.7805 | 0.1974 | 0.6687 | 0.3223 |
| (1,C) | 15 | 0.9428 | 0.0470 | 0.8224 | 0.0902 |
| (2,A) | 20 | | | 0.7244 | 0.1100 |
| (2,B) | 20 | 0.8916 | 0.0848 | 0.6124 | 0.1641 |
| (2,C) | 20 | 0.7630 | 0.2013 | 0.4579 | 0.4043 |
| (3,A) | 20 | | | 0.8606 | 0.1005 |
| (3,B) | 20 | 0.9082 | 0.0810 | 0.7551 | 0.1955 |
| (3,C) | 20 | 0.9082 | 0.0810 | 0.9297 | 0.0516 |

of the third session of the same case $(2, C)$, they could, in fact, be considered not qualified for being ground truth: the revision of the standards of the image acquisition procedure is suggested[2]. Related work on controls during the image acquisition time can be found in [4]. Note, that, in general, in spite of being related to descriptors completely different, the results presented in Tables 1 and 2 predict the classification results presented in Table 3 quite well.

## 3 Conclusions

The combination of conventional tools like the Expectation-Maximization Algorithm, the quadratic discriminant function and a classification window of optimal size has shown to be a suitable approach to segment images of psoriasis lesions. There are aspects related to the image data that are not irrelevant. This is, for instance, the case of the shadows, which clearly affect the quality of the classification results. For a correct lesions registration, it is required that thematic maps to be used to select the lesion patterns to be registered, -if they are automatically generated- have to contain a repeated pattern within and between sessions. This is, in general, not the case when the original data set is used. Illumination correction is required in order to improve the classification output. Hair and lesions occlusion are aspects to consider during the revision of the image acquisition standards.

On the other hand, results indicate that the parameters of the first image of each session could be used to segment the remaining images of the same session, when the situations mentioned before do not appear.

[2] A hair removal scheme is proposed in [1].

## Acknowledgments

To the SITE Project funded by a grant from the Danish Technical Research Foundation (Project Number *STVF* 56-00-0123) for supporting the present work. To the dermatologists Lone Skov and Bo Bang of the Gentofte Hospital of Denmark and to the anonymous patients, for their collaboration during the image acquisition sessions.

## Appendix

## A Expectation-Maximization Algorithm to each image

### A.1 The output of the first classification stage

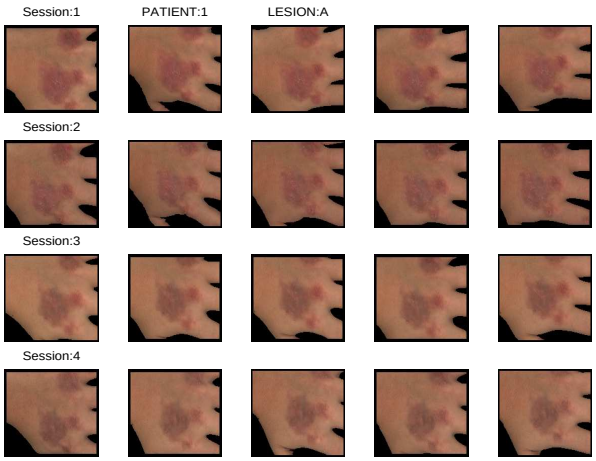


**Fig. 2.** Overlay of thematic maps with original images for (Patient 1, Lesion A).

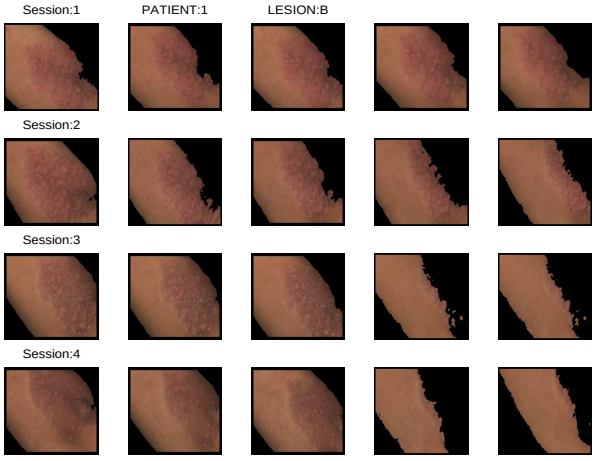


**Fig. 3.** Overlay of thematic maps with original images for (Patient 1, Lesion B).

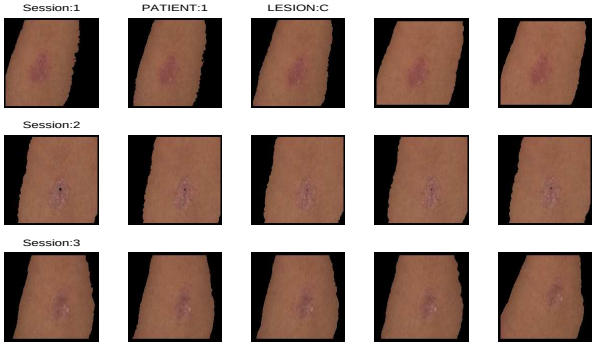


**Fig. 4.** Overlay of thematic maps with original images for (Patient 1, Lesion C).

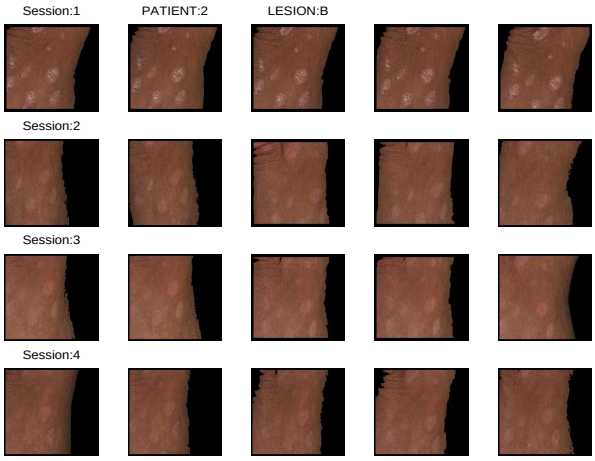


**Fig. 5.** Overlay of thematic maps with original images for (Patient 2, Lesion B).

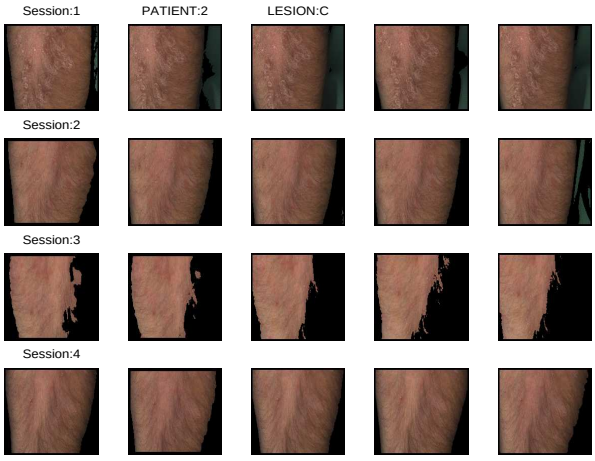


**Fig. 6.** Overlay of thematic maps with original images for (Patient 2, Lesion C).

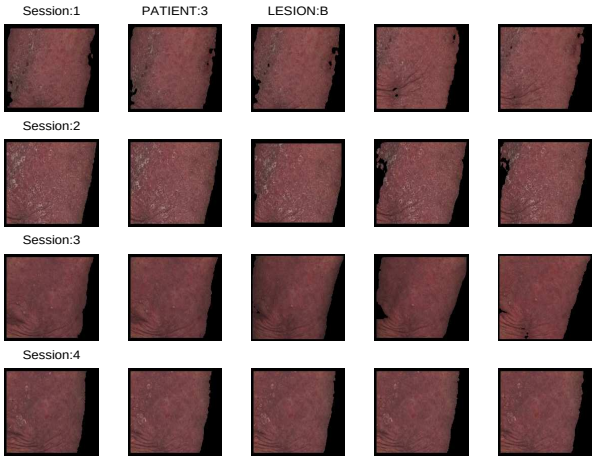


**Fig. 7.** Overlay of thematic maps with original images for (Patient 3, Lesion B).

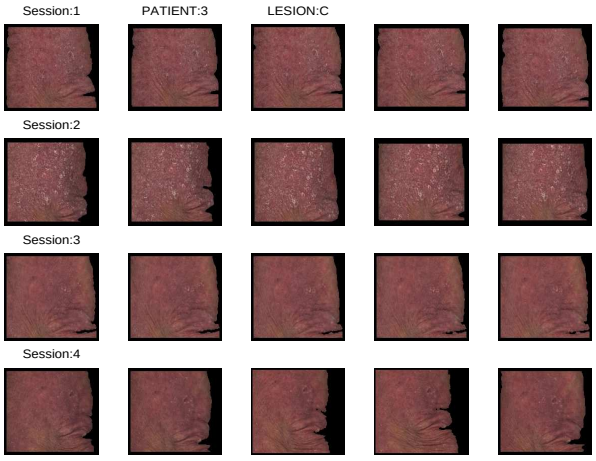


**Fig. 8.** Overlay of thematic maps with original images for (Patient 3, Lesion C).

### A.2 The output of the second classification stage

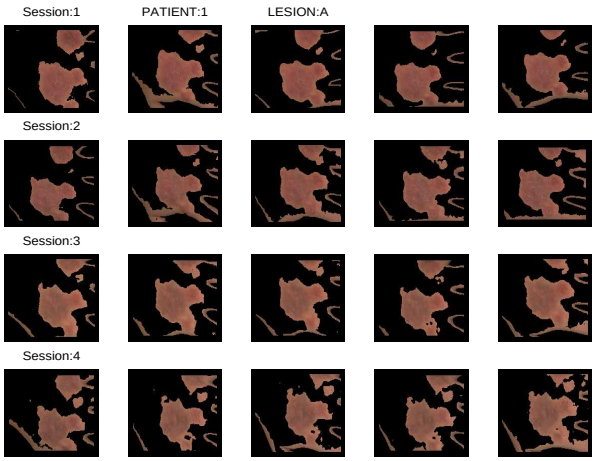


**Fig. 9.** Overlay of thematic maps with original images for (Patient 1, Lesion A).

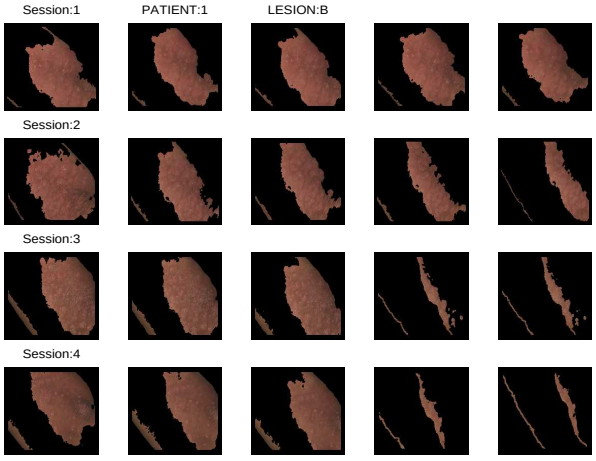


**Fig. 10.** Overlay of thematic maps with original images for (Patient 1, Lesion B).

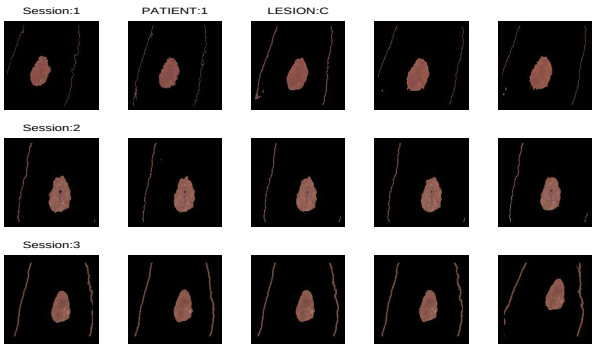


**Fig. 11.** Overlay of thematic maps with original images for (Patient 1, Lesion C).

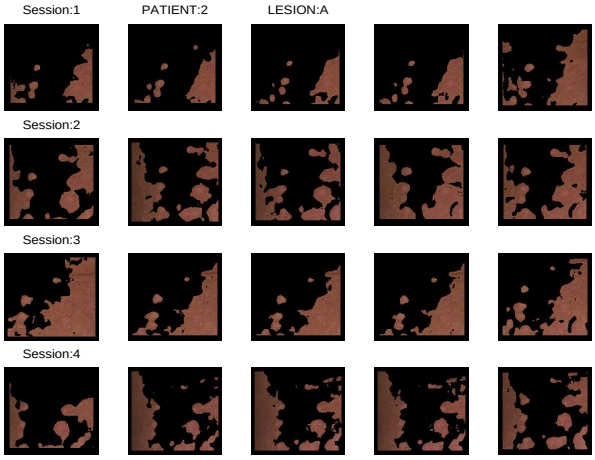


**Fig. 12.** Overlay of thematic maps with original images for (Patient 2, Lesion A).

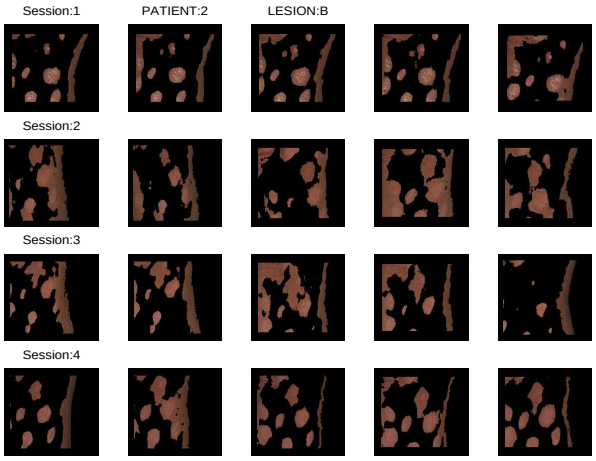


**Fig. 13.** Overlay of thematic maps with original images for (Patient 2, Lesion B).

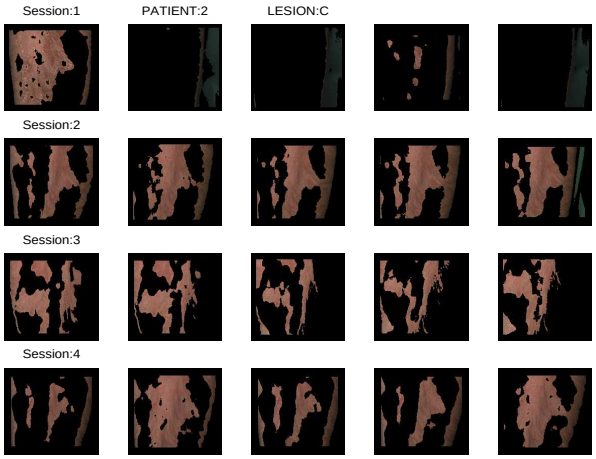


**Fig. 14.** Overlay of thematic maps with original images for (Patient 2, Lesion C).

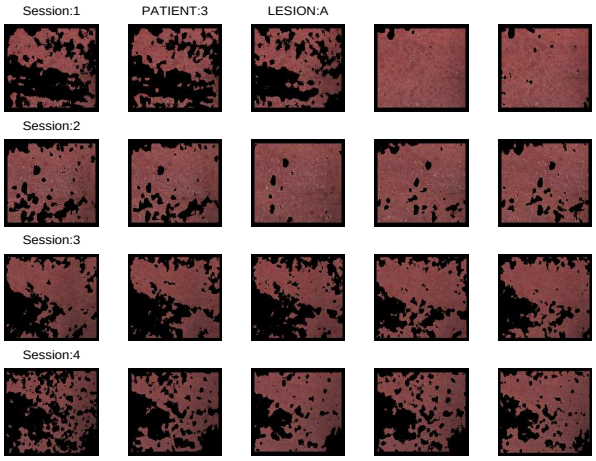


**Fig. 15.** Overlay of thematic maps with original images for (Patient 3, Lesion A).

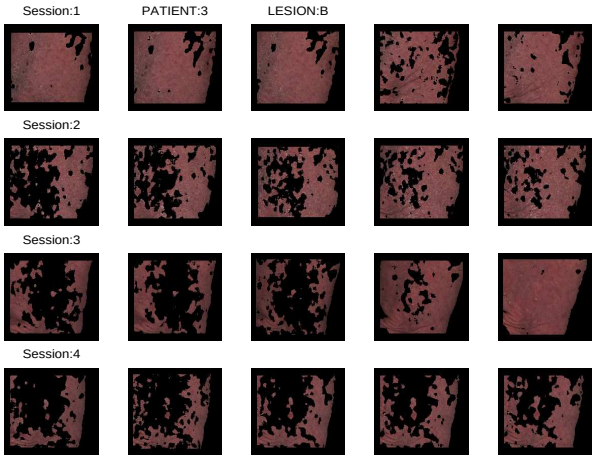


**Fig. 16.** Overlay of thematic maps with original images for (Patient 3, Lesion B).

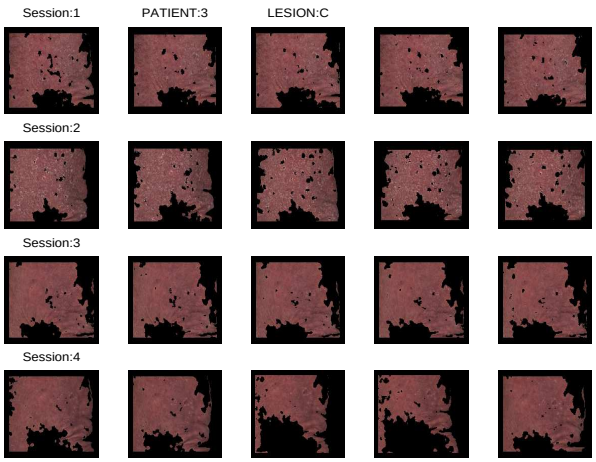


**Fig. 17.** Overlay of thematic maps with original images for (Patient 3, Lesion C).

## B Classification output analysis

In Table 4 the average correlation values of the normalized histogram of the normalized red band of each single image with the normalized histogram of the normalized red bands of the rest of the images of the same session are shown.

Details of the computation of each single cell value follow. The discrete correlations between pairs of normalized histograms of images of the same session was first computed:

$$c[h_{p,l,s,i,b}, h_{p,l,s,j,b}] = \frac{max(h_i \circ h_j)}{\sqrt{max(h_i \circ h_i) max(h_j \circ h_j)}} \tag{10}$$

where

$$(h_i \circ h_j)[n] = \sum_{k=-\infty}^{\infty} h_{p,l,s,i,b}[k], h_{p,l,s,j,b}[n+k] \tag{11}$$

where $h_{p,l,s,i,b} = h(nX_{p,l,s,i,b})$ and $h_{p,l,s,j,b} = h(nX_{p,l,s,j,b})$ are the normalized histograms of the normalized original images according to Equation 12:

$$nX_{p,l,s,c,b} = \frac{round(255. * (X_{p,l,s,c,b} - min(X_{p,l,s,c,b}))}{(max(X_{p,l,s,c,b}) - min(X_{p,l,s,c,b}))) + 1}. \tag{12}$$

The $nX$ images are the input to the Expectation-Maximization Algorithm. Each single cell value in Table 4 is the average correlation between each single image band and the rest of the images of the same session:

$$E[c[h_{p,l,s,i,b}, h_{p,l,s,:,b}]] = \frac{1}{n_c - 1}(\sum_{j=1} n_c c[h_{p,l,s,i,b}, h_{p,l,s,j,b}] - 1). \tag{13}$$

It has to be mentioned that the $X$ images used to compute these values were the "TIFF" format version of the original acquired "HIPS" format images, from which 10 rows and columns were removed from the borders, and then subsampled every four columns and rows.

Afterwards, with the same meaning as before, but now using the data of the region indicating skin Table 5 was generated.

**Table 4.** Average correlation values of the normalized histogram of the red band of each single image with the normalized histogram of the red band of the images that belong to the same session than that.

| Capture | $(1,A)$ | $(1,B)$ | $(1,C)$ | $(2,A)$ | $(2,B)$ | $(2,C)$ | $(3,A)$ | $(3,B)$ | $(3,C)$ |
|---|---|---|---|---|---|---|---|---|---|
| a1 | 0.8189 | 0.7957 | 0.8316 | 0.8024 | 0.8816 | 0.8191 | 0.8530 | 0.8086 | 0.8500 |
| a2 | 0.8516 | 0.8369 | 0.8481 | 0.7829 | 0.9027 | 0.8578 | 0.8353 | 0.7687 | 0.8919 |
| a3 | 0.8871 | 0.7765 | 0.8421 | 0.8143 | 0.9027 | 0.8346 | 0.8410 | 0.8082 | 0.8433 |
| a4 | 0.8388 | 0.7934 | 0.8404 | 0.7969 | 0.8819 | 0.8237 | 0.8585 | 0.7322 | 0.9027 |
| a5 | 0.8662 | 0.8251 | 0.8442 | 0.7990 | 0.8999 | 0.8376 | 0.8505 | 0.7361 | 0.8866 |
| b1 | 0.8929 | 0.7868 | 0.9063 | 0.8581 | 0.7149 | 0.8088 | 0.9177 | 0.8734 | 0.9052 |
| b2 | 0.8894 | 0.7624 | 0.9104 | 0.8867 | 0.7719 | 0.8190 | 0.8999 | 0.8406 | 0.9053 |
| b3 | 0.8327 | 0.8357 | 0.8765 | 0.8975 | 0.6648 | 0.7632 | 0.8835 | 0.9065 | 0.9124 |
| b4 | 0.8216 | 0.8242 | 0.8756 | 0.8855 | 0.7673 | 0.7753 | 0.9213 | 0.8603 | 0.8901 |
| b5 | 0.8722 | 0.8442 | 0.8693 | 0.8607 | 0.7373 | 0.7955 | 0.9136 | 0.9074 | 0.9157 |
| c1 | 0.8358 | 0.6901 | 0.8783 | 0.8683 | 0.8240 | 0.8644 | 0.8755 | 0.7955 | 0.8318 |
| c2 | 0.8855 | 0.7340 | 0.8633 | 0.8155 | 0.8275 | 0.8636 | 0.8865 | 0.7167 | 0.9079 |
| c3 | 0.8799 | 0.7445 | 0.8829 | 0.8387 | 0.8396 | 0.8308 | 0.8842 | 0.7560 | 0.9007 |
| c4 | 0.8680 | 0.7322 | 0.8535 | 0.8591 | 0.8252 | 0.8473 | 0.8428 | 0.7553 | 0.8504 |
| c5 | 0.7913 | 0.7310 | 0.8467 | 0.8613 | 0.8466 | 0.8613 | 0.8487 | 0.7257 | 0.9087 |
| d1 | 0.8026 | 0.6896 | | 0.9136 | 0.9044 | 0.7447 | 0.8956 | 0.9084 | 0.8189 |
| d2 | 0.8452 | 0.7172 | | 0.8950 | 0.8018 | 0.7256 | 0.8541 | 0.8490 | 0.8321 |
| d3 | 0.8689 | 0.7646 | | 0.9085 | 0.9078 | 0.8180 | 0.8614 | 0.9275 | 0.7794 |
| d4 | 0.8450 | 0.7534 | | 0.9122 | 0.9111 | 0.8344 | 0.8641 | 0.9278 | 0.8207 |
| d5 | 0.8623 | 0.7463 | | 0.7577 | 0.8953 | 0.8304 | 0.8905 | 0.9181 | 0.7860 |

**Table 5.** Average correlation values of the normalized histogram of the |B-G| band skin data of each single image with the normalized histogram of the |B-G| band skin data of the images that belong to the same session than that.

| Capture | $(1, A)$ | $(1, B)$ | $(1, C)$ | $(2, A)$ | $(2, B)$ | $(2, C)$ | $(3, A)$ | $(3, B)$ | $(3, C)$ |
|---|---|---|---|---|---|---|---|---|---|
| a1 | 0.6747 | 0.7358 | 0.7299 | 0.6528 | 0.6746 | 0.6895 | 0.6899 | 0.7057 | 0.8840 |
| a2 | 0.6866 | 0.4658 | 0.7075 | 0.7703 | 0.5487 | 0.6706 | 0.6906 | 0.6957 | 0.5348 |
| a3 | 0.6573 | 0.7413 | 0.7321 | 0.7358 | 0.6035 | 0.3545 | 0.5158 | 0.5983 | 0.8833 |
| a4 | 0.5051 | 0.7211 | 0.4225 | 0.7671 | 0.4346 | 0.7017 | 0.6030 | 0.7016 | 0.8812 |
| a5 | 0.7122 | 0.4212 | 0.4908 | 0.7272 | 0.6792 | 0.5224 | 0.6002 | 0.6973 | 0.8837 |
| b1 | 0.5920 | 0.4590 | 0.6418 | 0.6617 | 0.5848 | 0.3785 | 0.6737 | 0.3939 | 0.7666 |
| b2 | 0.5681 | 0.8282 | 0.7505 | 0.6029 | 0.4627 | 0.6018 | 0.6868 | 0.4781 | 0.7572 |
| b3 | 0.5227 | 0.8355 | 0.7631 | 0.6373 | 0.4604 | 0.5970 | 0.7039 | 0.5069 | 0.6391 |
| b4 | 0.6121 | 0.8588 | 0.6823 | 0.6230 | 0.6854 | 0.6525 | 0.5539 | 0.5619 | 0.7541 |
| b5 | 0.6000 | 0.8470 | 0.6929 | 0.6147 | 0.6996 | 0.6477 | 0.6828 | 0.5610 | 0.6415 |
| c1 | 0.2272 | 0.3549 | 0.6809 | 0.7719 | 0.4226 | 0.7562 | 0.6255 | 0.3718 | 0.4981 |
| c2 | 0.3616 | 0.3713 | 0.6213 | 0.5366 | 0.5482 | 0.7568 | 0.5076 | 0.4608 | 0.8747 |
| c3 | 0.6340 | 0.2635 | 0.6814 | 0.7889 | 0.5825 | 0.4534 | 0.6097 | 0.6005 | 0.8747 |
| c4 | 0.6382 | 0.4448 | 0.6356 | 0.7944 | 0.5925 | 0.5029 | 0.4510 | 0.6004 | 0.8747 |
| c5 | 0.6445 | 0.4449 | 0.6653 | 0.5660 | 0.5404 | 0.7504 | 0.4782 | 0.4266 | 0.8717 |
| d1 | 0.4177 | 0.4937 | | 0.7435 | 0.7712 | 0.7371 | 0.6559 | 0.4613 | 0.5106 |
| d2 | 0.5616 | 0.5653 | | 0.6118 | 0.7674 | 0.6809 | 0.6586 | 0.3015 | 0.6386 |
| d3 | 0.6008 | 0.5882 | | 0.7371 | 0.4272 | 0.7338 | 0.5211 | 0.4771 | 0.4917 |
| d4 | 0.5256 | 0.5784 | | 0.6323 | 0.5592 | 0.5559 | 0.5552 | 0.4761 | 0.6350 |
| d5 | 0.5877 | 0.5049 | | 0.7532 | 0.7739 | 0.4405 | 0.5085 | 0.4865 | 0.4552 |

# C Expectation-Maximization Algorithm to the first image of each section

**Table 6.** Kappa values $\kappa_{p,l,s,c,SKIN}$ of the classification outputs pointing skin using the Expectation-Maximization Algorithm for all the images of each sessions and for only the first image of each session.

| Capture | (1,A) | (1,B) | (1,C) | (2,B) | (2,C) | (3,B) | (3,C) |
|---|---|---|---|---|---|---|---|
| a1 | 1.0000 | 1.0000 | 1.0000 | 1.0000 | 1.0000 | 1.0000 | 1.0000 |
| a2 | 0.8716 | 0.9087 | 0.9846 | 0.9898 | 0.5030 | 0.8906 | 0.8906 |
| a3 | 0.8717 | 0.9039 | 0.9519 | 0.9904 | 0.3547 | 0.8463 | 0.8463 |
| a4 | 0.9786 | 0.8591 | 0.8795 | 0.9778 | 0.7077 | 0.9011 | 0.9011 |
| a5 | 0.8707 | 0.8332 | 0.8645 | 0.9429 | 0.3407 | 0.9081 | 0.9081 |
| b1 | 1.0000 | 1.0000 | 1.0000 | 1.0000 | 1.0000 | 1.0000 | 1.0000 |
| b2 | 0.8976 | 0.8192 | 0.9925 | 0.9734 | 0.8306 | 0.9995 | 0.9995 |
| b3 | 0.8775 | 0.8846 | 0.9792 | 0.8318 | 0.8233 | 0.8718 | 0.8718 |
| b4 | 0.9967 | 0.7799 | 0.9609 | 0.7741 | 0.8199 | 0.9251 | 0.9251 |
| b5 | 0.9891 | 0.7217 | 0.8593 | 0.9483 | 0.7019 | 0.9242 | 0.9242 |
| c1 | 1.0000 | 1.0000 | 1.0000 | 1.0000 | 1.0000 | 1.0000 | 1.0000 |
| c2 | 0.8714 | 0.9695 | 0.9328 | 0.9748 | 0.9033 | 0.9761 | 0.9761 |
| c3 | 0.8795 | 0.9355 | 0.9916 | 0.8448 | 0.8353 | 0.6875 | 0.6875 |
| c4 | 0.8368 | 0.4858 | 0.9433 | 0.8595 | 0.8788 | 0.7995 | 0.7995 |
| c5 | 0.9791 | 0.4762 | 0.9730 | 0.9195 | 0.8372 | 0.8946 | 0.8946 |
| d1 | 1.0000 | 1.0000 | | 1.0000 | 1.0000 | 1.0000 | 1.0000 |
| d2 | 0.9889 | 0.9759 | | 0.8966 | 0.7557 | 0.9712 | 0.9712 |
| d3 | 0.8823 | 0.9912 | | 0.7813 | 0.9807 | 0.9773 | 0.9773 |
| d4 | 0.9935 | 0.3843 | | 0.7408 | 0.9960 | 0.9776 | 0.9776 |
| d5 | 0.8878 | 0.5585 | | 0.8196 | 0.9400 | 0.9808 | 0.9808 |

**Table 7.** Kappa values $\kappa_{p,l,s,c,LESION}$ of the classification outputs pointing lesions using the Expectation-Maximization Algorithm for all the images of each sessions and for only the first image of each session.

| Capture | (1,A) | (1,B) | (1,C) | (2,A) | (2,B) | (2,C) | (3,A) | (3,B) | (3,C) |
|---|---|---|---|---|---|---|---|---|---|
| a1 | 1.0000 | 1.0000 | 1.0000 | 1.0000 | 1.0000 | 1.0000 | 1.0000 | 1.0000 | 1.0000 |
| a2 | 0.9122 | 0.9405 | 0.8717 | 0.9225 | 0.6138 | -0.2457 | 0.9812 | 0.9234 | 0.9072 |
| a3 | 0.9638 | 0.9483 | 0.7589 | 0.6850 | 0.8012 | -0.2721 | 0.7832 | 0.8886 | 0.9790 |
| a4 | 0.9245 | 0.9044 | 0.8364 | 0.9156 | 0.3756 | 0.1033 | 0.9351 | 0.6703 | 0.9382 |
| a5 | 0.9235 | 0.8978 | 0.7821 | 0.5262 | 0.8730 | -0.3099 | 0.9713 | 0.8554 | 0.9356 |
| b1 | 1.0000 | 1.0000 | 1.0000 | 1.0000 | 1.0000 | 1.0000 | 1.0000 | 1.0000 | 1.0000 |
| b2 | 0.8202 | 0.7448 | 0.9560 | 0.8165 | 0.8760 | 0.5099 | 0.9406 | 0.7988 | 0.9552 |
| b3 | 0.7717 | 0.7573 | 0.9104 | 0.5856 | 0.3908 | 0.5731 | 0.9093 | 0.7724 | 0.8910 |
| b4 | 0.7699 | 0.6711 | 0.8282 | 0.7383 | 0.6498 | 0.6802 | 0.7837 | 0.7712 | 0.8828 |
| b5 | 0.7684 | 0.6160 | 0.7628 | 0.8145 | 0.5664 | 0.6141 | 0.8890 | 0.7509 | 0.8627 |
| c1 | 1.0000 | 1.0000 | 1.0000 | 1.0000 | 1.0000 | 1.0000 | 1.0000 | 1.0000 | 1.0000 |
| c2 | 0.9449 | 0.9388 | 0.6406 | 0.6720 | 0.7954 | 0.8951 | 0.9111 | 0.9803 | 0.9822 |
| c3 | 0.9087 | 0.7187 | 0.9521 | 0.6532 | 0.4063 | 0.6506 | 0.9807 | 0.6579 | 0.9858 |
| c4 | 0.9334 | 0.2057 | 0.7234 | 0.7160 | 0.4181 | 0.5518 | 0.7379 | 0.2495 | 0.9844 |
| c5 | 0.9100 | 0.1663 | 0.8468 | 0.7315 | 0.6587 | 0.6263 | 0.8478 | 0.3693 | 0.9747 |
| d1 | 1.0000 | 1.0000 | | 1.0000 | 1.0000 | 1.0000 | 1.0000 | 1.0000 | 1.0000 |
| d2 | 0.9308 | 0.9565 | | 0.7249 | 0.5826 | 0.7522 | 0.6218 | 0.7755 | 0.9456 |
| d3 | 0.9606 | 0.9624 | | 0.5918 | 0.6335 | 0.6579 | 0.7978 | 0.8724 | 0.8503 |
| d4 | 0.9520 | 0.1097 | | 0.7147 | 0.6157 | 0.6424 | 0.7971 | 0.8483 | 0.8335 |
| d5 | 0.9515 | 0.1614 | | 0.7818 | 0.5416 | 0.8976 | 0.8822 | 0.8970 | 0.9665 |

## References


1. D. Chung and G. Sapiro. Segmenting skin lesions with partial differential equation based image processing algorithms. *IEEE International Conference on Image Processing*, 3(24):404–407, 2000.
2. W. Clarke, P. Lachenbruch, and B. Broffitt. How non-normality affects the quadratic discriminant function. *Communications in Statistics*, A8:1285–1301, 1979.
3. K. Conradsen. *En Introduktion til Statistik. Bind 2.* IMSOR DTH., Lyngby, 1984.
4. A. Gutenev, V. Skaldnev, and D. Varvel. Acquisiton-time quality control in digital dermatoscopy of skin lesions. *Computerized Medical Imaging and Graphics*, 25:495–499, 2001.
5. A. Hay. The derivation of global estimates from a confusion matrix. *International Journal of Remote Sensing*, 9(8):1395–1398, 1988.
6. G. Maletti and B. Ersbøll. Principal component analysis of psoriasis lesions images. Technical Report 5, Department of Informatics and Mathematical Modelling. Technical University of Denmark., Kgs. Lyngby. Denmark., March 2003.
7. G. Maletti, B. Ersbøll, and K. Conradsen. A contextual classifier that only requires one prototype pixel for each class. *IEEE Transactions on Nuclear Science*, 49(3):700–706, June 2002.
8. M. McGuire and H. Stone. Techniques for multiresolution image registration in the presence of occlusions. *IEEE Transactions on Geoscience and Remote Sensing*, 38(3):1476–1479, May 2000.
9. G. Rosenfield and K. Fitzpatrick-Lins. A coefficient of agreement as a measure of thematic classification accuracy. *Photogrammetric Engineering and Remote Sensing*, 52(2):223–227, February 1986.
10. S. Stehman. Thematic map accuracy assessment from the perspective of finite population sampling. *International Journal of Remote Sensing*, 16(3):589–593, 1995.
11. Y. Wang and T. Adali. *Signal Processing for Magnetic Resonance Imaging and Spectroscopy. Stocastic Model Based Image Analysis*, chapter 14, pages 1–34. 2000. (Topics in Biomedical Imaging Course Notes.).